Radiomics analysis allows for precise prediction of epilepsy in patients with low-grade gliomas

Zhenyu Liu[a,1], Yinyan Wang[b,d,1], Xing Liu[b,d,1], Yang Du[a], Zhenchao Tang[c], Kai Wang[b], Jingwei Wei[a], Di Dong[a], Yali Zang[a], Jianping Dai[b], Tao Jiang[b,d,*], Jie Tian[a,e,**]

[a] CAS Key Laboratory of Molecular Imaging, Institute of Automation, Beijing 100190, China
[b] Beijing Tiantan Hospital, Capital Medical University, Beijing 100050, China
[c] School of Mechanical, Electrical & Information Engineering, Shandong University, Weihai, Shandong Province 264209, China
[d] Beijing Neurosurgical Institute, Capital Medical University, Beijing 100050, China
[e] University of Chinese Academy of Sciences, Beijing 100080, China

ARTICLE INFO

ABSTRACT

Purpose: To investigate the association between imaging features and low-grade gliomas (LGG) related epilepsy, and to propose a radiomics-based model for the prediction of LGG-associated epilepsy.

Methods: This retrospective study consecutively enrolled 286 patients with LGGs (194 in the primary cohort and 92 in the validation cohort). T2-weighted MR images (T2WI) were used to characterize risk factors for LGG-related epilepsy: Tumor location features and 3-D imaging features were determined, following which the interactions between these two kinds of features were analyzed. Elastic net was applied to generate a radiomics signature combining key imaging features associated with the LGG-related epilepsy with the primary cohort, and then a nomogram incorporating radiomics signature and clinical characteristics was developed. The radiomics signature and nomogram were validated in the validation cohort.

Results: A total of 475 features associated with LGG-related epilepsy were obtained for each patient. A radiomics signature with eleven selected features allowed for discriminating patients with epilepsy or not was detected, which performed better than location and 3-D imaging features. The nomogram incorporating radiomics signature and clinical characteristics achieved a high degree of discrimination with area under receiver operating characteristic (ROC) curve (AUC) at 0.8769 in the primary cohort and 0.8152 in the validation cohort. The nomogram also allowed for good calibration in the primary cohort.

Conclusion: We developed and validated an effective prediction model for LGG-related epilepsy. Our results suggested that radiomics analysis may enable more precise and individualized prediction of LGG-related epilepsy.

1. Introduction

Low grade gliomas (LGG; World Health Organization grade II) (Scheithauer et al., 2008) is the most common type of primary brain tumor in young adults (Sanai et al., 2011). A majority of patients with LGG experience tumor-related epilepsy during the course of the disease (Chang et al., 2008; van Breemen et al., 2007). The impact of tumor-related epilepsy on quality of life for patients with LGG is profound due to life-threatening complications associated with epilepsy onset as well as long-term cognitive damage induced by the use of antiepileptic drugs (Chang et al., 2008; Maschio and Dinapoli, 2012; Weller et al., 2012).

Previous studies have suggested a number of risk factors for LGG-related epilepsy, including tumor location, peritumoral environment, and altered expression of the genes mediating neurotransmission(Huang et al., 2011; Pallud et al., 2014; van Breemen et al., 2007; Wang et al., 2015; Weller et al., 2012; You et al., 2012a), though the underlying etiology of such epilepsy remains to be elucidated.

Medical imaging, especially MRI, is indispensable in the investigation of the correlation between LGG and its secondary epilepsy for the ability to detect the brain activity noninvasively. Previous MRI-based demographic studies have mainly investigated the association between tumor location and related epilepsy, observing that involvement of

Table 1
Clinical characteristic of patients in the primary and validation cohorts.

Characteristics	Primary cohort		P	Validation cohort		P
	Epilepsy	No epilepsy		Epilepsy	No epilepsy	
Age, y, median (range)	37(15–64)	40(17–67)	0.197	42(17–66)	45(8–72)	0.249
Sex, M/F	81/55	29/29	0.219	41/19	16/16	0.085
MRI characteristics						
Tumor size, mean ± SD	73.5 ± 51.2	72.6 ± 58.3	0.867[a]	71.4 ± 54.5	73.2 ± 60.1	0.796[a]
Tumor pathology (%)						
Oligodendroglioma	14	10	0.178	7	1	0.166
IDH-mutant and 1p/19q-codeleted	10	5		4	1	
NOS	4	5		3	0	
Diffuse Astrocytoma	43	19	0.876	18	14	0.187
IDH-mutant	26	10		9	8	
IDH-wildtype	7	3		3	3	
NOS	10	6		6	3	
Oligoastrocytoma	79	29	0.299	35	17	0.631
NOS	79	29		35	17	
Radiomics score	0.8236 ± 0.29173	0.3540 ± 0.29742	< 0.001[a]	0.6715 ± 0.37991	0.3734 ± 0.28888	< 0.001[a]

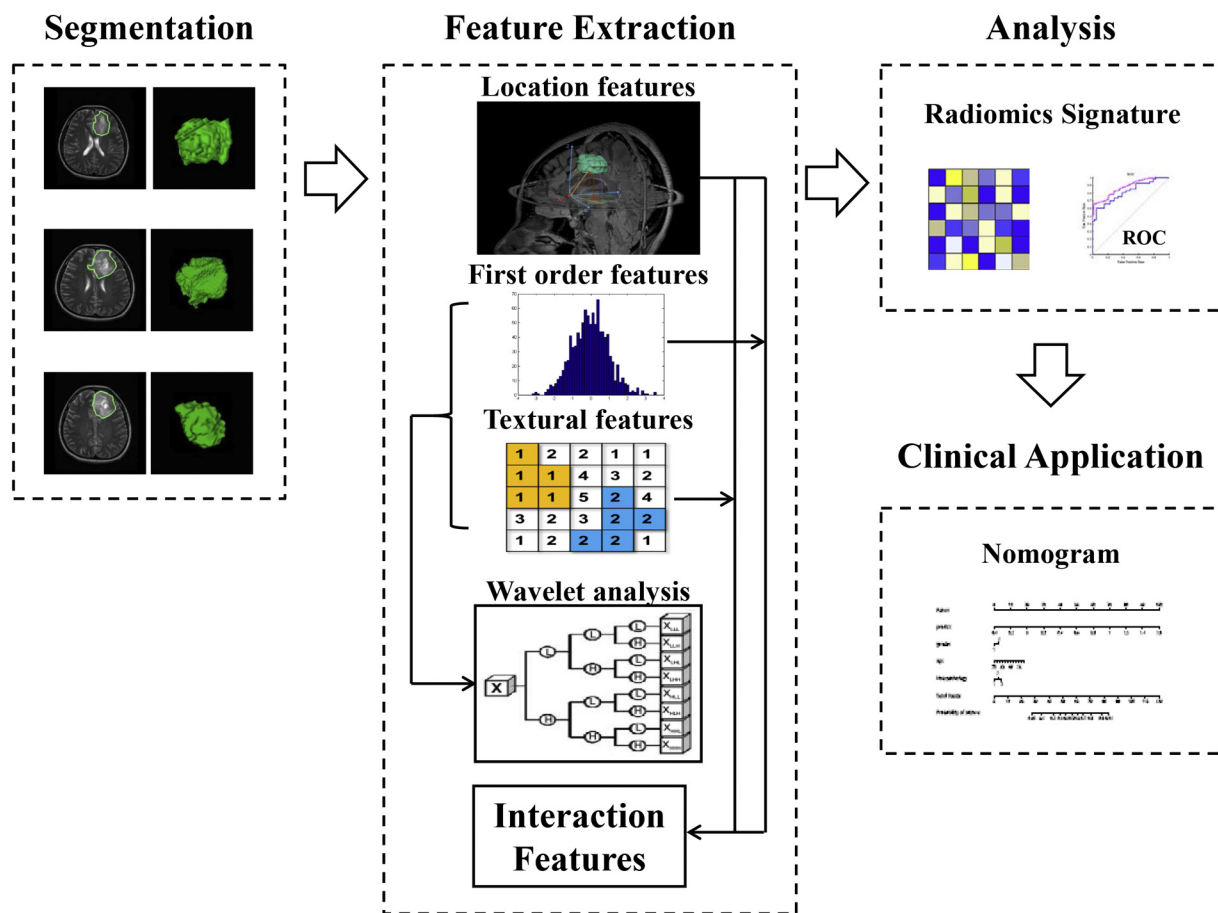NOS, not otherwise specified.

[a] Result of *t*-test.

Fig. 1. Flowchart of the study. With manually segmented tumor, we first extracted 474 quantitative imaging features, including location features, 3-D imaging features, and their interactions from masked presurgical T2-weighted MRIs. The general view of the feature extraction algorithm was shown in the figure. Then, feature selection was applied on the extracted features with E-net and a radiomics signature was constructed with the selected features. Finally, radiomics signature and clinical characteristics were incorporated into a nomogram for individually prediction.

eloquent (Pallud et al., 2014), cortical (You et al., 2012b), and insular regions (Lee et al., 2010) is linked with the epilepsy occurrence in LGG patients. Further, a voxel-based imaging analysis provided a probabilistic risk atlas of glioma-related epilepsy (Wang et al., 2015). However, tumor location may be one among a number of comprehensive risk factors for LGG-related epilepsy, and few researchers have focused on the association between quantitative imaging features of intrinsic tumor lesions and epilepsy occurrence.

Advances in pattern recognition tools have facilitated the development of radiomics, which involves the extraction of a large number of quantitative features from medical images in order to determine relationships among these features and a given underlying

Fig. 2. Tumor masking and quantitative location information. Masks of the brain tumors were drawn on each patient's T2-weighted images in native space by two board-certified neuroradiologists. We set up a coordinate system with the anterior commissure (AC) as the origin point. Polar coordinates (r, θ, and Φ) of the centroid of the tumor were identified as location features.

pathophysiology. Radiomics analysis of such large imaging data sets has been successfully employed in the field of oncology (Kumar et al., 2012; Lambin et al., 2012), and there is increasing interest within the field in defining association maps between tumor heterogeneity and imaging features (Gillies et al., 2015). By extracting high-throughput quantitative features from routine acquired CT images, radiomics enables the noninvasive profiling of tumor heterogeneity (Aerts et al., 2014). Recent advances in radiomics have enabled oncologists to deliver more personalized medical care with regard to tumor detection, phenotypic subtypes, and assessment of therapeutic responses (Altazi et al., 2015; Huang et al., 2016; Itakura et al., 2015; Li et al., 2015). Given the potential of radiomics analysis for providing a more reliable estimation of risk for LGG-related epilepsy, the development of a multivariable prediction model combining quantitative imaging features is a necessary step in enhancing care and treatment for this patient population.

In the present study, we collected T2-weighted MR Images from 286 patients with LGG and subsequently constructed a radiomics signature by combining multiple imaging biomarkers selected from tumor location features and 3-D imaging features as well as possible interactions among these features. Furthermore, we developed a radiomics nomogram that incorporated both the radiomics signature and clinical characteristics for individual prediction of LGG-related epilepsy risk.

2. Methods

2.1. Patients

A total of 286 patients with LGGs who had been surgically treated at Beijing Tiantan Hospital between September 2008 and March 2015 were consecutively enrolled in this retrospective study. *There was a partial overlap*

(< 50%) between the datasets in our previous study (Wang et al., 2015) *and that in the present study.* All included cases met the following criteria: histopathologically confirmed grade II gliomas according to World Health Organization criteria 2016 (patients without diagnostic molecular testing was designated as not otherwise specified categories) (Tang et al., 2007), presurgical T2-weighted MRIs of the brain, and no prior craniotomy or stereotactic biopsy. All enrolled patients were listed in chronological order, the first 194 patients were identified as primary cohort and other 92 patients were identified as validation cohort. The clinical characteristics of the patients, including age, gender, tumor location, and history of epilepsy occurrence are summarized in Table 1. Our study was approved by the ethics committee of Beijing Tiantan Hospital. The flow chart of the study is illustrated in Fig. 1.

2.2. Evaluation of tumor-related epilepsy

Patients were considered to have experienced tumor-related epilepsy when a history of at least one seizure with the presence of an enduring alteration (i.e., LGG) in the brain (Fisher et al., 2005) was reported. History of epilepsy and seizure types (generalized and focal) were evaluated by an epileptologist based on the presentation of the epilepsy according to the classification and terminology of the International League Against Epilepsy (ILAE) (Fisher et al., 2017).

2.3. Brain imaging and tumor masking

MRI scans were obtained on a Magnetom Trio 3.0T scanner (Siemens, Erlangen, Germany) using a 12-channel receive-only head coil. The T2-weighted image parameters were as follows: repetition time = 5800 ms; echo time = 110 ms; flip angle = 150 degrees; 24 slices; field of view = 240×188 mm^2; voxel size = $0.6 \times 0.6 \times 5.0$ mm^3; matrix = 384×300. Tumors were traced directly on the brain MRIs using MRIcron (http://www.mccauslandcenter.sc.edu/mricro/mricron). Masks of the brain tumors were drawn on each patient's T2-weighted images in native space by two board-certified neuroradiologists, which were blinded to the patients' clinical information. Areas that produced abnormally hyperintense signals on T2-weighted images were identified as LGG tumor areas. The tumor masks were combined when there was less than a 5% discrepancy between the individual masks identified by the two neuroradiologists. When a > 5% discrepancy existed between these two masks, the masks utilized were determined by a senior neuroradiologist.

2.4. Extraction of quantitative imaging features

We first generated a "tumor cube" covering the area of the tumor using the tumor mask and T2-weighted images for each patient. Then, three groups of quantitative features were extracted depending on the tumor cube.

Group I: Location features. For the extraction of tumor location features, a coordinate system with anterior commissure (AC) as the origin point was constructed in Montreal Neurological Institute (MNI) space. The data of each patient was registered to the MNI template, and the polar coordinates of the centroid of the tumor and the distance from

Table 2
Performance of the different features.

Metrics	AUC		Accuracy	
	Primary cohort	Validation cohort	Primary cohort	Validation cohort
Location (95%)	0.7567 (0.7146 to 0.7962)	0.6541 (0.6237 to 0.7065)	70.10% (64.95% to 74.74%)	66.30% (61.96% to 69.56%)
3-D Imaging features (95%)	0.7857 (0.7563 to 0.8364)	0.7612 (0.7072 to 0.7921)	75.26% (72.16% to 77.32%)	70.65% (66.30% to 73.91%)
Radiomics signature (95%)	0.8754 (0.8265 to 0.9213)	0.8162 (0.7318 to 0.9005)	79.38% (76.22% to 82.22%)	75.00% (71.74% to 78.26%)

Abbreviations: AUC, area under ROC curve.

Table 3

Quantitative image features extracted for prediction.

Class		Features	Numbers
Location	First order statistics	Polar coordinate (r, θ, Φ), cityblock, chebychev, mahalanobis, and cosine distance	7
	Shape based features	Energy, Entropy, Kurtosis, Mean, Maximum, Minimum, Median, Range, RMS, Skewness, Variance, Standard deviation, Uniformity	13
	Textural features	Compactness I, Compactness II, sphericity, spherical disproportion, Surface to volume ratio (SVR), Volume, Surface area	7
	Wavelet features	Gray level co-occurrence matrix (GLCM)'s:	25
		Energy, Entropy, Correlation, Contrast, Homogeneity, Variance, Sum average, Autocorrelation, Cluster shade, Cluster tendency, Probability, Inverse variance;	
		Gray level run-length matrix (GLRL)'s:	
		Short Run Emphasis (SRE), Long Run Emphasis (LRE), Gray Level Non-Uniformity (GLN), Run Length Non-Uniformity (RLN), Run Percentage (RP), Low Gray Level Run Emphasis (LGLRE), High Gray Level Run Emphasis (HGLRE), Short Run Low Gray Level Emphasis (SRLGLE), Short Run High Gray Level Emphasis (SRHGLE), Long Run High Gray Level Emphasis (LRHGLE), Long Run Low Gray Level Emphasis (LRLGLE);	
		Fractal Dimension (FD), Average Fractal Dimension (FDa)	
		3D "Coiflet 1" wavelet transform on images with 8 decompositions: LLL, LLH, LHL, LHH, HLL, HLH, HHL, HHH; Then re-calculate the first order statistics features and textural features.	304
Interaction features		Statistically significant (p < 0.05) seizure related interactions between location features and 3-D imaging features without wavelet	119
Total			475

AC to the centroid of the tumor were calculated. Seven location features were extracted, including the polar coordinates (*r*, *θ*, and *Φ*) of the centroid of the tumor and Cityblock distance, Chebyshev distance, Mahalanobis distance, and Cosine distance from the AC to the centroid of the tumor (See Fig. 2).

Group II: Three dimensional imaging features. A total of 349 3-D imaging features of the tumor, including 13 first order statistical features (Energy, Entropy, Kurtosis, Mean, Maximum, Minimum, Median, Range, RMS, Skewness, Variance, Standard deviation, and Uniformity), seven shape- and size-based features (Compactness I, Compactness II, sphericity, spherical disproportion, Surface to volume ratio (SVR), Volume, Surface area), 25 texture features (GLCM: Energy, Entropy, Correlation, Contrast, Homogeneity, Variance, Sum average, Autocorrelation, Cluster shade, Cluster tendency, Probability, and Inverse variance, and GLRL: Short Run Emphasis (SRE), Long Run Emphasis (LRE), Gray Level Non-Uniformity (GLN), Run Length Non-Uniformity (RLN), Run Percentage (RP), Low Gray Level Run Emphasis (LGLRE), High Gray Level Run Emphasis (HGLRE), Short Run Low Gray Level Emphasis (SRLGLE), Short Run High Gray Level Emphasis (SRHGLE), Long Run High Gray Level Emphasis (LRHGLE), Long Run Low Gray Level Emphasis (LRLGLE), Fractal Dimension (FD), Average Fractal Dimension (FDa)), and 304 wavelet features recalculated of the first order statistics features and textural features on images after 3D "Coiflet 1" wavelet transform.

Group III: Interaction features between location features and 3-D imaging features without wavelet. The products of each location feature and each 3-D imaging feature without wavelet were detected as interaction features. 119 statistically significant (*p < 0.05*) epilepsy-related interactions calculated using linear regression were used as potential predictors in the development of the multivariable model.

The detailed information and formula to detect the 475 MR-based imaging features was described in the supplement (See Table 3).

2.5. Feature selection and prediction

To reduce any type of over-fitting or bias in the multivariate analysis, the Elastic net (*E*-Net) was used in order to select the most predictive features from the primary data set. E-net aimed at selecting the model that achieved the best trade-off between goodness of fit and model complexity by minimizing the residual sum of squares of estimating errors plus the penalty term, which made it suitable for a regression model. It can be seen that the E-net penalty was a weighted sum of the least absolute shrinkage and selection operator (LASSO) penalty and ridge penalty. In the present study, models including a small number of features were regarded to be of lower complexity.

Glmnet (Friedman et al., 2010) (http://statweb.stanford.edu/~tibs/lasso.html), which could provide efficient procedures for fitting the entire LASSO or *E*-net regularization path for linear regression, was used in order to obtain the key features.

The epileptic status of the patients (1 for epileptic and 0 for non-epileptic) was estimated with the imaging features using the following model:

$$y = sigmoid\left(\sum_{i=1}^{n} \beta_i x_i + \beta_0 + \varepsilon \right)$$

where y was the epileptic status of the patients; n was the number of features, here n = 475; x_i (i = 1, 2, …, n) was the independent parameter; β_i (i = 0, 1, 2, …, n) was the coefficient, and ε was the error term. By forcing many parameters to zero, feature selection can be performed. The aim was to minimize the following cost function:

$$\sum_{i=1}^{N} \left(y_i - sigmoid\left(\sum_{j=1}^{n} \beta_j x_{ij} - \beta_0 \right) \right)^2 + \lambda \sum_{j=1}^{n} (\alpha |\beta_j| + 0.5(1 - \alpha)(\beta_j)^2)$$

where y_i was the epileptic status of the ith patients; N was the number of patients; x_{ij} was the jth feature of the ith patients; and λ and α were tuning parameters. We selected λ and α in the E-net model used 10-fold cross-validation via minimum criteria. Specifically, the values for the parameter α were restricted between 0 and 1 in steps of 0.1, and the values of λ were restricted between 0.001 and 1. Features with non-zero coefficients resulted by the optimal λ and α were selected as potential predictors for further analysis. A radiomics signature was calculated for each patient via a linear combination of selected features that were weighted by their respective coefficients. Based on the constructed radiomics signature, the AUC, and classification accuracy were calculated as metrics used to assess the quantitative discrimination performance of the model in the primary cohort and validation cohort.

2.6. Development of an individualized prediction model

Multivariable logistic regression analysis was conducted with the following clinical information: age, sex, histopathology and radiomics signature. A model for epilepsy detection was developed on the basis of the primary cohort. Backward step-wise selection was applied by using the likelihood ratio test with Akaike's information criterion as the stopping rule (Collins et al., 2015; Sauerbrei et al., 2011).

Based on the multivariable logistic analysis in the primary cohort, a radiomics nomogram for LGG-related epilepsy detection was built to provide a quantitative tool for clinical use. Calibration curves were
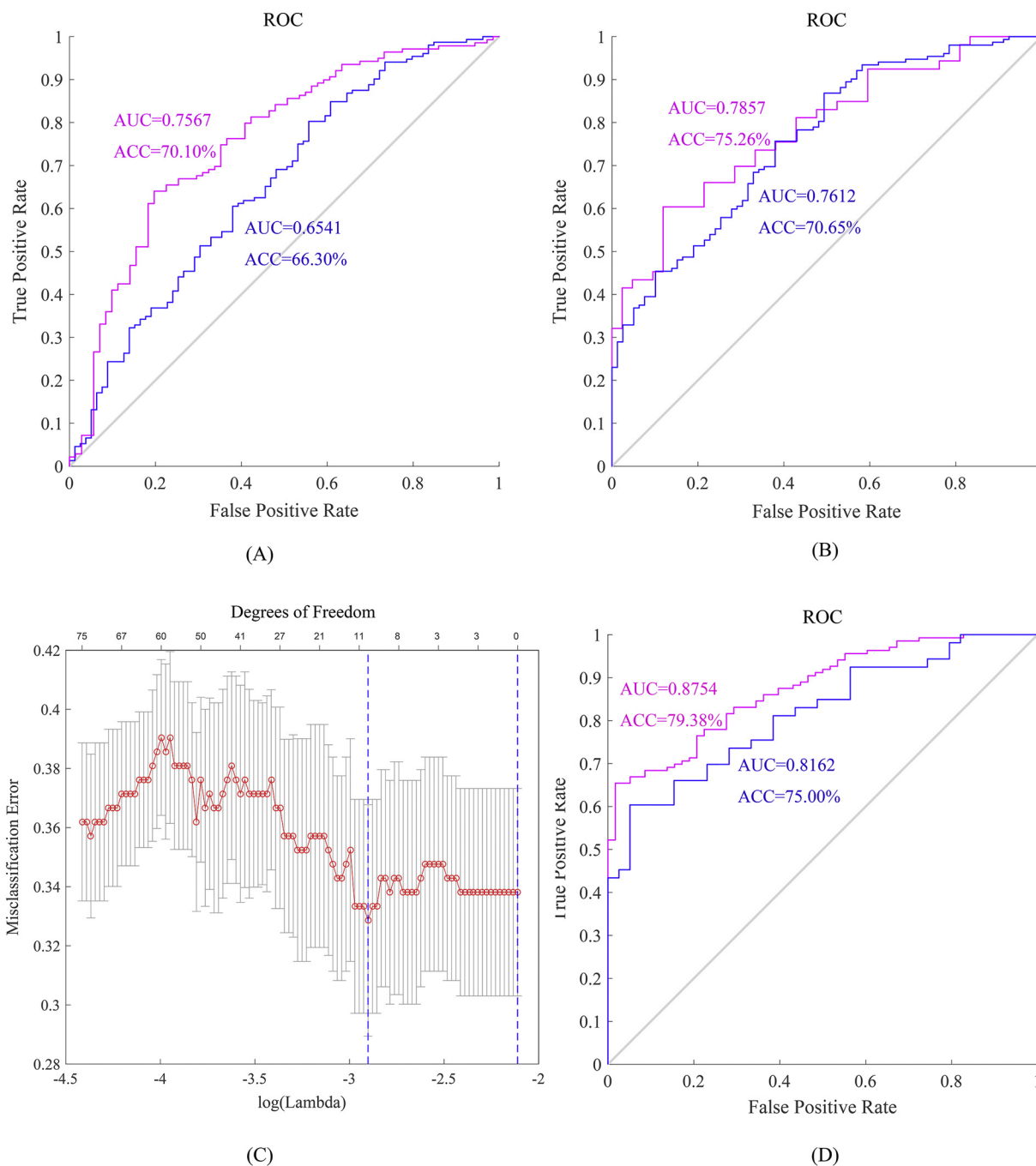
Fig. 3. ROC curve of multivariate analysis with location features (A) and 3-D imaging features (B) (the pink lines represent the performance in the primary cohort and the blue lines represent the performance in the validation cohort). (C) Tuning parameter (λ) selection in the E-net used 10-fold cross-validation via minimum criteria. (D) ROC curve of radiomics signature (the pink lines represent the performance in the primary cohort and the blue lines represent the performance in the validation cohort).

plotted to assess the calibration of the radiomics nomogram, accompanied with the Hosmer-Lemeshow test. (A significant test statistic implies that the model does not calibrate perfectly.) *The calibration curves described the agreement between the estimated risk of epilepsy and the actual rate of epilepsy. The calibration curve can be drawn by plotting $\widehat{P}$ on the x-axis while $P_c = [1 + exp - (\gamma_0 + \gamma_1 L)]^{-1}$ on the y-axis. Here, P_c represented the actual probability of epilepsy, and $L = logit(\widehat{P})$, $\widehat{P}$ was the estimated risk of epilepsy, γ_0 was corrected intercept, and γ_1 was slope estimate.* And Harrell's C-index was measured to quantify the discrimination performance of the radiomics nomogram. The nomogram was subjected to bootstrapping validation (1000 bootstrap resamples) to detect a relatively corrected performance.

3. Results

3.1. Demographic and clinical data

There were no significant differences between the two cohorts in epilepsy prevalence ($p = 0.406$). Patients with epilepsy accounted for 70.1% and 65.2% in the primary and validation cohort. There were also no significant differences in the clinical characteristics between the epilepsy group and non-epilepsy group, either within the primary and validation cohorts, which justified their use as training and testing cohorts.
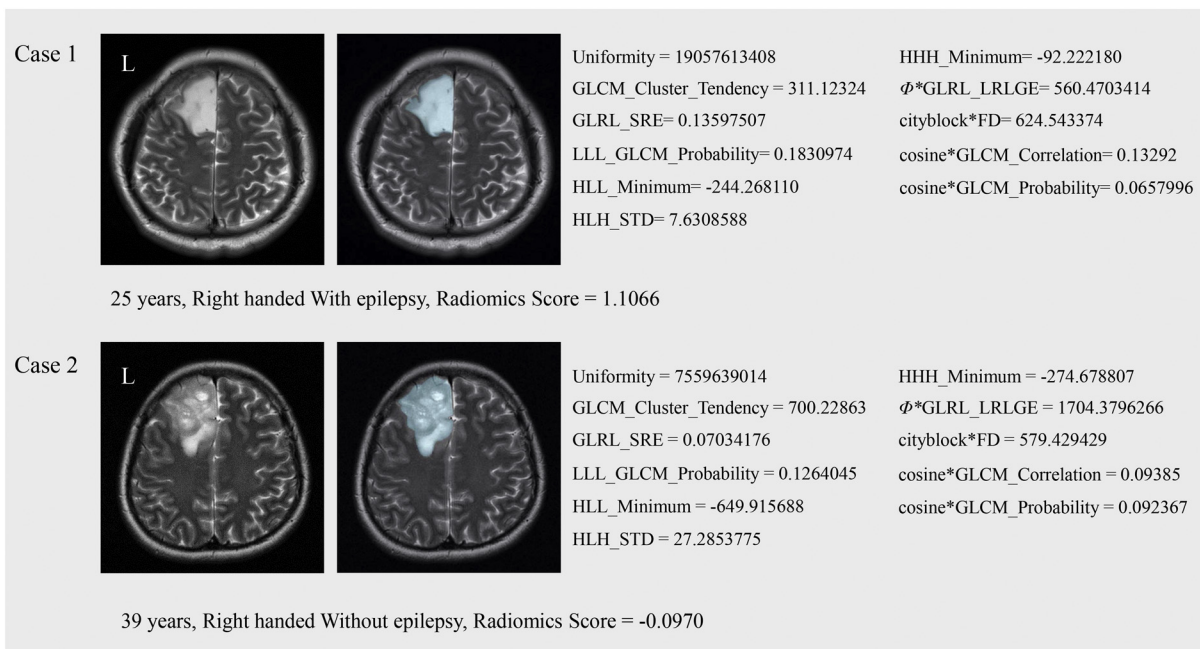
Case 1

Uniformity = 19057613408
GLCM_Cluster_Tendency = 311.12324
GLRL_SRE= 0.13597507
LLL_GLCM_Probability= 0.1830974
HLL_Minimum= -244.268110
HLH_STD= 7.6308588

HHH_Minimum= -92.222180
Φ*GLRL_LRLGE= 560.4703414
cityblock*FD= 624.543374
cosine*GLCM_Correlation= 0.13292
cosine*GLCM_Probability= 0.0657996

25 years, Right handed With epilepsy, Radiomics Score = 1.1066

Case 2

Uniformity = 7559639014
GLCM_Cluster_Tendency = 700.22863
GLRL_SRE = 0.07034176
LLL_GLCM_Probability = 0.1264045
HLL_Minimum = -649.915688
HLH_STD = 27.2853775

HHH_Minimum = -274.678807
Φ*GLRL_LRLGE = 1704.3796266
cityblock*FD = 579.429429
cosine*GLCM_Correlation = 0.09385
cosine*GLCM_Probability = 0.092367

39 years, Right handed Without epilepsy, Radiomics Score = -0.0970

Fig. 4. T2-weighted images with tumor masks for two cases with LGG. Top row: images in a patient who was classified into the epilepsy group with an epilepsy risk score of 1.1066. Bottom row: images in a patient who was classified into the non- epilepsy group with a radiomics score of −0.0970. (Patients with radiomics score > 0 would be classified into epilepsy group, while patients with radiomics score < 0 would be classified into non-epilepsy group).
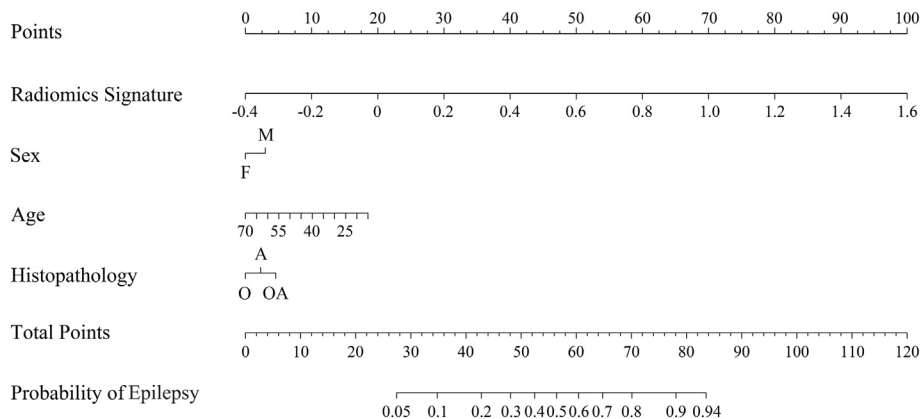

Fig. 5. Developed radiomics nomogram. The radiomics nomogram was developed in the primary cohort, with the radiomics signature and clinical characteristics (including sex, age, and histopathology) incorporated. With the nomogram, probability of epilepsy for each patient could be calculated on the basis of logistic regression formula using the total points.

3.2. Feature selection and Radiomics signature building

E-net was performed to detect key features for prediction (Fig. 3C). *epileptic (λ.) was selected in the E-net with 10-fold cross-validation via minimum criteria in the primary cohort. The misclassification error was plotted versus log (λ). A λ value of 0.055 was chosen (minimum criteria) according to 10-fold cross-validation. The α value of 0.8 was chosen with minimum criteria in the loop from 0 to 1 in steps of 0.1.* Eleven features with non-zero coefficients were consequently selected from all 475 features, including Uniformity, GLCM_Cluster_Tendency, GLRL_SRE, LLL_GLCM_Probability, HLL_Minimum, HLH_STD, HHH_Minimum, Φ*GLRL_LRLGE, cityblock*FD, cosine*GLCM_Correlation, and cosine*GLCM_Probability. Radiomics signature was obtained with a linear combination of these features achieved using E-net. The predictive ability of the radiomics signature was interpreted according to the ROC curve (Fig. 3D). It achieved a performance with classification accuracy = 79.38%, AUC = 0.8754 in the primary cohort and classification accuracy = 75.00%, AUC = 0.8162 in the validation cohort (See Table 2).

3.3. Performance of Radiomics nomogram

Nomogram for epilepsy detection was developed combining clinical characteristics and radiomics signature (Fig. 5). The calibration curve of the nomogram for the probability of epilepsy demonstrated a well agreement in the primary cohort (Fig. 6). The Hosmer-Lemeshow test yielded nonsignificant statistics ($p = 0.229$), which suggested that there was no departure from the perfect fit. The C-index of the nomogram was 0.8769 (95% CI: 0.8303–0.9235) within the primary cohort and 0.8152 (95% CI: 0.7311–0.8993) within the validation cohort.

4. Discussion

In the present study, we aimed to elucidate a radiomics signature combining MRI features associated with LGG-related epilepsy. Our findings demonstrated that MR-based radiomics features may reflect epilepsy susceptibility in LGG patients. The radiomics signature successfully stratified patients according to their epilepsy risk. Incorporating the radiomics signature and clinical characteristics into a nomogram further facilitated the prediction of epilepsy risk.

Recent developments in the field of radiomics have allowed for the
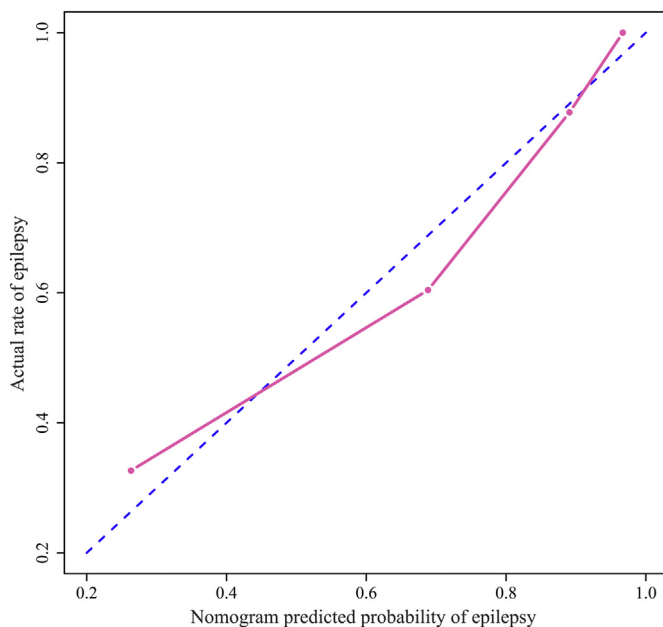
Fig. 6. Calibration curve of the radiomics nomogram in the primary cohort.

extraction of high-throughput imaging features, enabling oncologists to derive more precise information with regard to individual patient conditions and treatment options (Lambin et al., 2013). A number of studies have developed radiomics-based predictive models for various clinical characteristics, including survival outcomes (Aerts et al., 2014), lymph node metastasis (Huang et al., 2016), and treatment responses (Nie et al., 2016). Moreover, some researchers have suggested that radiomics analysis may be able to predict the clinical characteristics and molecular background of brain tumors by combining various quantitative MRI features (Gevaert et al., 2015; Itakura et al., 2015). As tumor-related epilepsy was among the most important clinical characteristics associated with LGGs, we constructed a radiomics signature that combined three-dimensional imaging features, tumor locations, and their interactions with *E*-net. The radiomics signature achieved a relatively high discrimination accuracy and AUC in both primary and validation cohorts, suggesting that the radiomics analysis of the present study was effective in detecting LGG-related epilepsy. Additionally, the established nomogram benefits for the clinical application of rapid epilepsy prediction. Our model incorporated radiomics signature and clinical characteristics, the risk LGG-related epilepsy could be individually and accurately evaluated.

For the realization of radiomics analysis, effective imaging features are necessary for further prediction. Several 3-D imaging features were selected as key features in the present study, which have been applied in previous radiomics studies (Aerts et al., 2014; Itakura et al., 2015). These features not only described the intuitive sense of tumors but also provided abundant information on tumor heterogeneity and microenvironments (Gillies et al., 2015). *In the present study, the most predictive features of epilepsy status were selected based on the E-net model, and the biological correlations between these features and epilepsy occurrence could also be revealed preliminarily. For instance, the results of the present study indicated that Uniformity, a radiological indicator for the consistency of the images, which reflected tumor homogeneity (Aerts et al., 2014), could serve as a predictive factor of the epilepsy status. As known to us, higher tumor homogeneity was usually associated with lower tumor malignancy, and lower tumor malignancy may be accompanied with increased epilepsy risk based on clinical findings. Thus, we can speculate that, higher Uniformity indicated higher epilepsy risk, which was consistent with the result of the present study* (Fig. 4).

Tumor location is another influential factor associated with

epilepsy. A probabilistic risk atlas of LGG-related epilepsy has been illustrated (Wang et al., 2015). However, previous studies (Lee et al., 2010; Pallud et al., 2014; You et al., 2012b) were mainly based on segmented and masked tumor lesions. While the imaging information inside the tumor area was ignored, and the location information was used as categorized data. Considering that differences in epilepsy susceptibility may exist for different sub-regions of a brain lobe, quantitative descriptions of tumor location are necessary. We accordingly constructed a coordinate system in which the tumor location was accurately described using the polar coordinates of the centroid of the tumor as well as the distances. This quantitative description provided more detailed tumor location information and allowed us to incorporate tumor location into the estimation model of epilepsy risk.

In addition, the interactions between tumor location and other risk factors were considered in the present prediction model, as tumors of the same size in various locations (or tumors in the same location of various sizes) may be associated with different degrees of epilepsy risk. Therefore, we investigated the interactive effects between 3-D imaging features and tumor location. Reasonably, the interactions between tumor location and 3-D imaging features were significantly associated with epilepsy ($p < 0.05$) in the multivariate classification model. Our results demonstrate that the interactions provided significant contributions to the epilepsy prediction model, and that inconsistent increases in epilepsy risk were accompanied by the growth of gliomas in various locations. The observed susceptibility to tumor-related epilepsy was also in accordance with the probabilistic risk of epilepsy determined using voxel-based mapping (Wang et al., 2015). Our findings indicate that interaction features may provide additional important information for the prediction of LGG-related epilepsy.

Radiomics integrates comprehensive imaging features, though it is important to note that inclusion of unrelated features may result in over-fitting or bias in the predictive model. To exclude redundant features and promote the creation of an effective prediction model, we preserved 11 key features that preferentially contributed to epilepsy prediction and achieved a relatively good prediction performance. We utilized E-net, which is suitable for the regression of high-dimensional data and computationally more efficient and less prone to overfitting (Sauerbrei et al., 2007), as the feature selection method in the current study. The results demonstrated that selected key feature achieved the classification performance.

The prediction results of the present study, when taken with those of previous studies, also suggested that the combination of imaging features with location information may allow for a construction of an improved prediction model. While location was only one of the risk factors for LGG related epilepsy, the other 468 features used in the present study may provide additional information of epilepsy risk and help the prediction of epilepsy occurrence.

The present study also possesses some limitations. First, stereotactic electroencephalographic data was not available for localization of epilepsy originations. In this study, the diagnosis of epilepsy was based on clinical presentation. As patients with LGG are often referred for surgery shortly following diagnosis, many are unfortunately unable to undergo electroencephalography prior to surgery. Second, the divergence of tumor histopathology with epilepsy remains controversial and was consequently not considered in this study. Despite the above limitations, this study quantitatively detected radiomics features and the machine learning classification was well validated. *A deep learning model was encouraged to be applied in future studies with multicenter collection and a larger sample of data.*

5. Conclusions

In conclusion, we identified an effective radiomics signature combining a series of imaging features, which allowed for the effective noninvasive prediction of LGG-related epilepsy. Furthermore, our results suggest that radiomics analysis may be an effective method for the

individualized evaluation and management of LGG-related epilepsy.

Conflict of interest

Acknowledgements

Appendix A. Supplementary data

Supplementary data to this article can be found online at https://doi.org/10.1016/j.nicl.2018.04.024.

References

Aerts, H.J.W.L., Velazquez, E.R., Leijenaar, R.T.H., Parmar, C., Grossmann, P., Carvalho, S., Bussink, J., Monshouwer, R., Haibe-Kains, B., Rietveld, D., Hoebers, F., Rietbergen, M.M., Leemans, C.R., Dekker, A., Quackenbush, J., Gillies, R.J., Lambin, P., 2014. Decoding tumour phenotype by noninvasive imaging using a quantitative radiomics approach. Nat. Commun. 5, 4006.

Altazi, B., Fernandez, D., Zhang, G., Biagioli, M., Moros, E., Moffitt, H.L., 2015. SU-EJ-258: prediction of cervical cancer treatment response using radiomics features based on F18-FDG uptake in PET images. Med. Phys. 42, 3326.

Chang, E.F., Potts, M.B., Keles, G.E., Lamborn, K.R., Chang, S.M., Barbaro, N.M., Berger, M.S., 2008. Seizure characteristics and control following resection in 332 patients with low-grade gliomas. J. Neurosurg. 108, 227–235.

Collins, G.S., Reitsma, J.B., Altman, D.G., Moons, K.G.M., Grp, T., 2015. Transparent reporting of a multivariable prediction model for individual prognosis or diagnosis (TRIPOD): the TRIPOD statement. Eur. Urol. 67, 1142–1151.

Fisher, R.S., van Emde Boas, W., Blume, W., Elger, C., Genton, P., Lee, P., Engel Jr., J., 2005. Epileptic seizures and epilepsy: definitions proposed by the International League Against Epilepsy (ILAE) and the International Bureau for Epilepsy (IBE). Epilepsia 46, 470–472.

Fisher, R.S., Cross, J.H., French, J.A., Higurashi, N., Hirsch, E., Jansen, F.E., Lagae, L., Moshe, S.L., Peltola, J., Roulet Perez, E., Scheffer, I.E., Zuberi, S.M., 2017. Operational classification of seizure types by the International League Against Epilepsy: position paper of the ILAE Commission for Classification and Terminology. Epilepsia 58, 522–530.

Friedman, J., Hastie, T., Tibshirani, R., 2010. Regularization paths for generalized linear models via coordinate descent. J. Stat. Softw. 33, 1–22.

Gevaert, O., Mitchell, L.A., Achrol, A.S., Xu, J., Echegaray, S., Steinberg, G.K., Cheshier, S.H., Napel, S., Zaharchuk, G., Plevritis, S.K., 2015. Glioblastoma multiforme: exploratory radiogenomic analysis by using quantitative image features. Radiology 276, 313.

Gillies, R.J., Kinahan, P.E., Hricak, H., 2015. Radiomics: images are more than pictures, they are data. Radiology 151169.

Huang, L., You, G., Jiang, T., Li, G.L., Li, S.W., Wang, Z.C., 2011. Correlation between tumor-related seizures and molecular genetic profile in 103 Chinese patients with low-grade gliomas: a preliminary study. J. Neurol. Sci. 302, 63–67.

Huang, Y.Q., Liang, C.H., He, L., Tian, J., Liang, C.S., Chen, X., Ma, Z.L., Liu, Z.Y., 2016. Development and validation of a radiomics nomogram for preoperative prediction of lymph node metastasis in colorectal cancer. J. Clin. Oncol. 34, 2157–2164.

Itakura, H., Achrol, A.S., Mitchell, L.A., Loya, J.J., Liu, T., Westbroek, E.M., Feroze, A.H., Rodriguez, S., Echegaray, S., Azad, T.D., Yeom, K.W., Napel, S., Rubin, D.L., Chang, S.D., Harsh, G.R.t., Gevaert, O., 2015. Magnetic resonance image features identify glioblastoma phenotypic subtypes with distinct molecular pathway activities. Sci. Transl. Med. 7 (303ra138).

Kumar, V., Gu, Y.H., Basu, S., Berglund, A., Eschrich, S.A., Schabath, M.B., Forster, K., Aerts, H.J.W.L., Dekker, A., Fenstermacher, D., Goldgof, D.B., Hall, L.O., Lambin, P., Balagurunathan, Y., Gatenby, R.A., Gillies, R.J., 2012. Radiomics: the process and the challenges. Magn. Reson. Imaging 30, 1234–1248.

Lambin, P., Rios-Velazquez, E., Leijenaar, R., Carvalho, S., van Stiphout, R.G.P.M., Granton, P., Zegers, C.M.L., Gillies, R., Boellard, R., Dekker, A., Aerts, H.J.W.L., Consortium, Q.-C., 2012. Radiomics: extracting more information from medical images using advanced feature analysis. Eur. J. Cancer 48, 441–446.

Lambin, P., van Stiphout, R.G., Starmans, M.H., Rios-Velazquez, E., Nalbantov, G., Aerts, H.J., Roelofs, E., van Elmpt, W., Boutros, P.C., Granone, P., Valentini, V., Begg, A.C., De Ruysscher, D., Dekker, A., 2013. Predicting outcomes in radiation oncology--multifactorial decision support systems. Nat. Rev. Clin. Oncol. 10, 27–40.

Lee, J.W., Wen, P.Y., Hurwitz, S., Black, P., Kesari, S., Drappatz, J., Golby, A.J., Wells 3rd, W.M., Warfield, S.K., Kikinis, R., Bromfield, E.B., 2010. Morphological characteristics of brain tumors causing seizures. Arch. Neurol. 67, 336–342.

Li, H., Lan, L., Drukker, K., Perou, C., Giger, M., 2015. TU-AB-BRA-08: radiomics in the analysis of breast cancer heterogeneity on DCE-MRI. Med. Phys. 42, 3588.

Maschio, M., Dinapoli, L., 2012. Patients with brain tumor-related epilepsy. J. Neuro-Oncol. 109, 1–6.

Nie, K., Shi, L., Chen, Q., Hu, X., Jabbour, S., Yue, N., Niu, T., Sun, X., 2016. Rectal cancer: assessment of neoadjuvant chemoradiation outcome based on radiomics of multiparametric MRI. Clin. Cancer Res. 22 (21), 5256–5264.

Pallud, J., Audureau, E., Blonski, M., Sanai, N., Bauchet, L., Fontaine, D., Mandonnet, E., Dezamis, E., Psimaras, D., Guyotat, J., Peruzzi, P., Page, P., Gal, B., Parraga, E., Baron, M.H., Vlaicu, M., Guillevin, R., Devaux, B., Duffau, H., Taillandier, L., Capelle, L., Huberfeld, G., 2014. Epileptic seizures in diffuse low-grade gliomas in adults. Brain 137, 449–462.

Sanai, N., Chang, S., Berger, M.S., 2011. Low-grade gliomas in adults. J. Neurosurg. 115, 948–965.

Sauerbrei, W., Royston, P., Binder, H., 2007. Selection of important variables and determination of functional form for continuous predictors in multivariable model building. Stat. Med. 26, 5512–5528.

Sauerbrei, W., Boulesteix, A.L., Binder, H., 2011. Stability investigations of multivariable regression models derived from low- and high-dimensional data. J. Biopharm. Stat. 21, 1206–1231.

Scheithauer, B.W., Fuller, G.N., VandenBerg, S.R., 2008. The 2007 WHO classification of tumors of the nervous system: controversies in surgical neuropathology. Brain Pathol. 18, 307–316.

Tang, Y., Zhang, Y.Q., Huang, Z., 2007. Development of two-stage SVM-RFE gene selection strategy for microarray expression data analysis. IEEE/ACM Trans. Comput. Biol. Bioinform. 4, 365–381.

van Breemen, M.S., Wilms, E.B., Vecht, C.J., 2007. Epilepsy in patients with brain tumours: epidemiology, mechanisms, and management. Lancet Neurol. 6, 421–430.

Wang, Y.Y., Qian, T.Y., You, G., Peng, X.X., Chen, C., You, Y.P., Yao, K., Wu, C.X., Ma, J., Sha, Z.Y., Wang, S.Y., Jiang, T., 2015. Localizing seizure-susceptible brain regions associated with low-grade gliomas using voxel-based lesion-symptom mapping. Neuro-Oncology 17, 282–288.

Weller, M., Stupp, R., Wick, W., 2012. Epilepsy meets cancer: when, why, and what to do about it? Lancet Oncol. 13, e375–382.

You, G., Huang, L., Yang, P., Zhang, W., Yan, W., Wang, Y., Bao, Z., Li, S., Li, S., Li, G., Jiang, T., 2012a. Clinical and molecular genetic factors affecting postoperative seizure control of 183 Chinese adult patients with low-grade gliomas. Eur. J. Neurol. 19, 298–306.

You, G., Sha, Z.Y., Yan, W., Zhang, W., Wang, Y.Z., Li, S.W., Sang, L., Wang, Z., Li, G.L., Li, S.W., Song, Y.J., Kang, C.S., Jiang, T., 2012b. Seizure characteristics and outcomes in 508 Chinese adult patients undergoing primary resection of low-grade gliomas: a clinicopathological study. Neuro-Oncology 14, 230–241.